Monthly Notices
of the
ROYAL ASTRONOMICAL SOCIETY

MNRAS **450,** 3771–3777 (2015) doi:10.1093/mnras/stv861

New age–metallicity diagnostic diagram for the Washington photometric system

Andrés E. Piatti[1,2]★ and Gabriel I. Perren[2,3]

[1]*Observatorio Astronómico, Universidad Nacional de Córdoba, Laprida 854, 5000, Córdoba, Argentina*
[2]*Consejo Nacional de Investigaciones Científicas y Técnicas, Av. Rivadavia 1917, C1033AAJ, Buenos Aires, Argentina*
[3]*Facultad de Ciencias Astronómicas y Geofísicas, Universidad Nacional de La Plata, Paseo del Bosque s/n, 1900 La Plata, Argentina*

Accepted 2015 April 15. Received 2015 April 15; in original form 2015 March 18

ABSTRACT

The age calibration of the Washington δT_1 index is mainly used to estimate ages of star clusters older than 1 Gyr and no age–metallicity degeneracy effect is considered. We have profusely exploited synthetic T_1 versus $C - T_1$ colour magnitude diagrams to explore the intrinsic behaviour of the δT_1 index. The analysis shows that δT_1 varies with age and metal content as well. In general, the dependence on age weakens for ages greater than ∼6 Gyr, and is even less sensitive to age as the metallicity decreases. For ages younger than ∼5 Gyr, δT_1 shows a strong correlation with both age and metallicity. The δC index – defined as δT_1 for the C passband – is also a combined measurement of age and metallicity. We introduce a new age–metallicity diagnostic diagram, δT_1 versus $\delta C - \delta T_1$, which can unambiguously provide age and metallicity estimates, simultaneously. The new procedure can be used to derive ages from 1 up to 13 Gyr and metallicities [Fe/H] from −2.0 up to +0.5 dex, and is independent of the cluster reddening and distance modulus. It solves the constraints found in the δT_1 index and surpasses the performance of the standard giant branch metallicity method. All these features make the diagnostic diagram a powerful tool for estimating accurate ages as well as metallicities.

Key words: techniques: photometric.

1 INTRODUCTION

Geisler et al. (1997, hereafter G97) provided a calibration for the magnitude difference (δ) between the giant branch clump in intermediate-age star clusters (the horizontal branch in old clusters) and the main sequence turn-off as a function of the cluster age for the Washington photometric system. In particular, they used the T_1 versus $C - T_1$ colour magnitude diagram (CMD) (effective wavelengths: $C \sim 3900$ Å, $T_1 \sim 6300$ Å; Canterna 1976) of six known star clusters (ages $\gtrsim$1 Gyr) to measure δT_1 and fitted those values with the clusters' ages (see their fig. 5 and equation 4). δT_1 emulated the former δV index defined by Phelps, Janes & Montgomery (1994). Using this calibration, G97 first searched for old star clusters in the Large Magellanic Cloud; the 25 candidates analysed were of intermediate age (1–3 Gyr). Since then, the δT_1 index has been employed successively to estimate the ages of star clusters in the Milky Way (e.g. Piatti, Clariá & Ahumada 2004), in both Magellanic Clouds (e.g. Bica et al. 1998; Piatti et al. 2001) and to derive ages for the so-called representative stellar population of galactic star fields (e.g. Piatti, Geisler & Mateluna 2012), among others.

The age calibration of the δT_1 index is based on CT_1 photometry of NGC 2213 and ESO 121-SC03 in the Large Magellanic Cloud and the Galactic open clusters NGC 1245, Tombaugh 2, M67 and NGC 6791. At the very least, the calibration needs revision, since updated ages and metallicities for the calibration clusters are available. For instance, Anthony-Twarog, Twarog & Mayer (2007) derived an age of (7.0 ± 1.0) Gyr for NGC 6791 ([Fe/H] = (+0.42 ± 0.05) dex; Heiter et al. 2014), whereas a value of 10 Gyr was used by G97. Except for ESO 121-SC03 ([Fe/H] = (−0.93 ± 0.20) dex; Olszewski et al. 1991), all of these calibration clusters are considerably more metal-rich than [Fe/H] approximately −0.5 dex. In addition, the solar abundance cluster M67 plays a pivotal role in the calibration, as it is the only cluster in the 2–9 Gyr range. Secondly, thinking about the impact that the adopted cluster fundamental parameters can have on the former age calibration of the δT_1 index, it seems necessary to enlarge the cluster sample to support a robust relationship and to allow an analysis of the possible metallicity sensitivity and the effect any such sensitivity might have on the derived ages. Nowadays, however, a representative sample of clusters with age and metallicity values distributed well along the known cluster age/metallicity regime and

★ E-mail: andres@oac.uncor.edu

with Washington CT_1 photometry is not available. Given the usefulness that δT_1 has shown in the literature as a cluster age indicator, the above constraints seriously blur its full scope.

Fortunately, synthetic cluster CMDs are powerful tools for probing the genuine performance of δT_1 as an age indicator and for disentangling any metallicity dependence. This is because they can accurately reproduce CMDs of clusters of any age and metallicity, bearing in mind the fraction of binaries, the cluster initial mass function (IMF), the cluster mass, as well as photometric uncertainties and completeness effects, etc. (Popescu, Hanson & Elmegreen 2012; Casagrande & VandenBerg 2014). In this sense, synthetic cluster CMDs have the advantage of representing those of calibration clusters with ages and metallicities derived on a homogeneous scale. Indeed, we have taken advantage of the recently developed Automated Stellar Cluster Analysis package (ASteCA,[1] Perren, Vázquez & Piatti 2015), as we describe in Section 2 of this work, to exploit profusely a large number of synthetic cluster CMDs. From the outcomes of this comprehensive analysis, we present in Section 3 a new age–metallicity diagnostic diagram that involves δ values for the C and T_1 passbands. The proposed technique can estimate ages and metallicities for clusters older than 1 Gyr, independent of their reddening and distance moduli. Section 4 analyses the performance of the new procedure in the light of published accurate age and metallicity values as well as the different age and metallicity calibration in the Washington system. Finally, Section 5 summarizes our main results.

2 SYNTHETIC COLOUR-MAGNITUDE DIAGRAMS

Synthetic stellar populations have usually been generated to study the astrophysical properties of different stellar populations through the comparison of their respective CMDs (e.g. Romeo et al. 1989; Hernandez, Valls-Gabaud & Gilmore 1999; Monteiro, Dias & Caetano 2010). The recovery of the star formation history of galaxies (Rubele et al. 2012), the study of the extended main sequence turn-off phenomenon in star clusters (Correnti et al. 2014), and the estimation of star cluster parameters (Donati et al. 2015) have been topics of astrophysical interest approached by synthetic CMD analyses. Likewise, synthetic CMDs offer the possibility to explore in detail the behaviour of different photometric indices in terms of astrophysical quantities (Catelan et al. 2014), to predict the range of distinct fundamental properties of star clusters (Popescu & Hanson 2014) as well as to assess in advance the performance of astronomical instruments (Kerber et al. 2009).

To revise the δT_1 age calibration and its possible dependence on the metal content, we employed the ASteCA suite of functions to generate synthetic CMDs of star clusters covering ages from 1.0 up to 12.6 Gyr and metallicities in the range [Fe/H] = (−2.0–+0.5) dex. ASteCA was designed as a new set of open-source tools for the objective and automatic analysis of large cluster data sets. The code includes functions for cluster structure analysis, luminosity function curves, integrated colour estimates statistically cleaned of field star contamination, a Bayesian membership assignment algorithm, and a synthetic cluster-based best isochrone matching method to estimate simultaneously cluster properties (age, metallicity, distance, reddening, mass and binarity). Perren et al. (2015) showed that it does not introduce any biases or new correlations between the various derived cluster parameter values.

[1] http://asteca.github.io/

The steps by which a synthetic cluster for a given set of age, [Fe/H], distance modulus $m - M$ and reddening $E(B - V)$ values is generated by ASteCA is as follows: (i) A theoretical isochrone is picked and densely interpolated so it contains 1000 points throughout its entire length, including the most evolved stellar phases. (ii) The isochrone is shifted in colour and magnitude according to the $E(B - V)$ and $m - M$ values to emulate the effects these extrinsic parameters have over the isochrone in the CMD. At this stage the synthetic cluster can be objectively identified as a unique point in the four-dimensional space of parameters ($E(B - V)$, $m - M$, age and metallicity). (iii) The isochrone is trimmed down to a faintest magnitude according to the limiting magnitude thought to be reached. (iv) An IMF is sampled in the mass range [$\sim$ 0.01–100] $M_\odot$ up to a total mass value $M_{\rm total}$ provided via an input data file that ensures the evolved CMD regions are properly populated. Currently, ASteCA lets the user choose between three IMFs (Kroupa, Tout & Gilmore 1993; Chabrier 2001; Kroupa 2002) but there is no limit to the number of distinct IMFs that can be added. The distribution of masses is then used to obtain a properly populated synthetic cluster by keeping one star in the interpolated isochrone for each mass value in the distribution. (v) A random fraction of stars are assumed to be binaries, set by default to 50 per cent (von Hippel 2005), with secondary masses drawn from a uniform distribution between the mass of the primary star and a fraction of it given by a mass ratio parameter set to 0.7. Both quantities can be modified through the input data file. (vi) Appropriate magnitude completeness and exponential photometric error functions are finally applied to the synthetic cluster.

We used the theoretical isochrones computed by Bressan et al. (2012) using extensive tabulations of bolometric corrections with uncertainties $\sim$0.001 mag for the C and T_1 filters, the IMF of Chabrier (2001), and a cluster mass as a function of the cluster age given by the expression $\log(M_{\rm total}\,M_\odot) = 1.8 \times \log({\rm age yr}^{-1}) - 12.8$ (Baumgardt et al. 2013; de Grijs, Goodwin & Anders 2013; Piatti 2014) to keep not only the main sequence turn-off (MSTO) but also the red clump (RC), which was similarly populated as those of known low-mass clusters. We considered no binarity effect, since it has been shown that binary stars can broaden the MSTO region (Li et al. 2012; Li, de Grijs & Deng 2013; Jiang, Han & Li 2014), in contrast with our aim of determining the sensitivity of the MSTO to age and metallicity. Fig. 1 shows some examples of the resulting synthetic CMDs. Note that the theoretical isochrones of Bressan et al. (2012) have a very satisfactory agreement with another known set of isochrones for the Washington system computed by Lejeune & Schaerer (2001) (e.g. Piatti et al. 2003, and references therein).

3 THE δT_1 INDEX

We measured the difference in magnitude between the MSTO and the RC in the generated synthetic CMDs following the precepts of Phelps et al. (1994, see their fig. 1), as G97 also used in their definition of δT_1. The synthetic cluster CMDs allowed us to estimate the errors involved in measuring δT_1. We found that an uncertainty between 0.05 and 0.10 mag typically affects the measurements of δT_1, and can reach a few hundredths of magnitude for some of the youngest clusters in our synthetic sample because of the shape of their MSTOs. Fig. 2 (upper left-hand panel) shows the resulting δT_1 values as a function of age for six different metallicity levels (coloured line scale). As can be seen, the relationship of δT_1 with age varies with the metal content as well. In general, the trend of δT_1 with age weakens (it changes to a smaller slope) for ages larger than $\sim$6 Gyr, and is even less sensitive to age as the stellar population

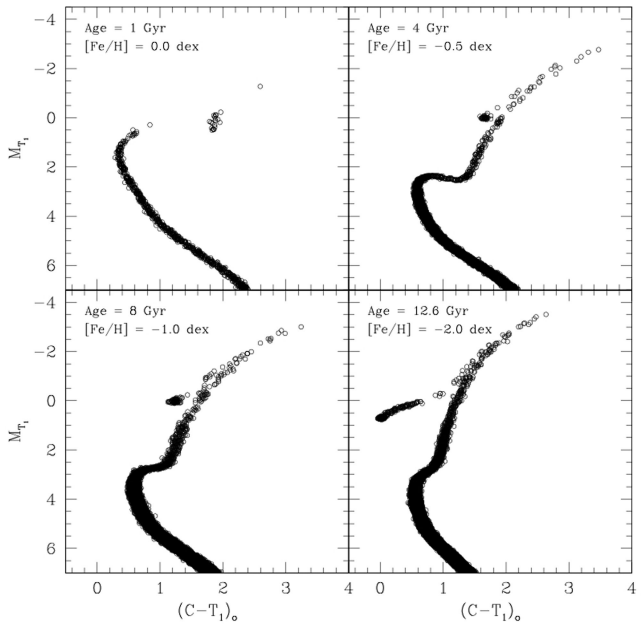

Figure 1. Examples of synthetic CMDs produced using the ASTECA suite of functions.

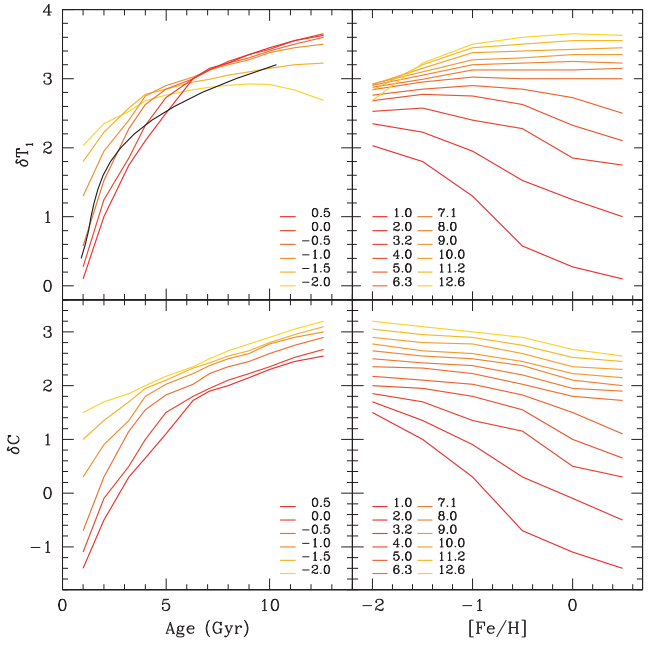

Figure 2. Relationship of δC and δT_1 indices with age for different [Fe/H] (dex) values (left-hand panels) and with metallicity for different ages (Gyr) (right-hand panels). The black curve in the upper left-hand panel corresponds to the G97 calibration.

becomes more metal-poor ([Fe/H] $\lesssim -1.0$ dex). This means that δT_1 is not a good indicator of age independent of metallicity for old and metal-poor clusters. For ages younger than ∼5 Gyr, δT_1 shows a strong correlation with both age and metallicity.

We included in Fig. 2 (upper left-hand panel) the relationship obtained by G97 as a solid black line. For ages younger than 3 Gyr, they used three calibration clusters, two of them (NGC 2243 and Tombaugh 2) have an average spectroscopic metallicity of [Fe/H] = (−0.4 ± 0.10) dex. Their δT_1 versus age relationship roughly matches the synthetic one for [Fe/H] = −0.5 dex. On the other

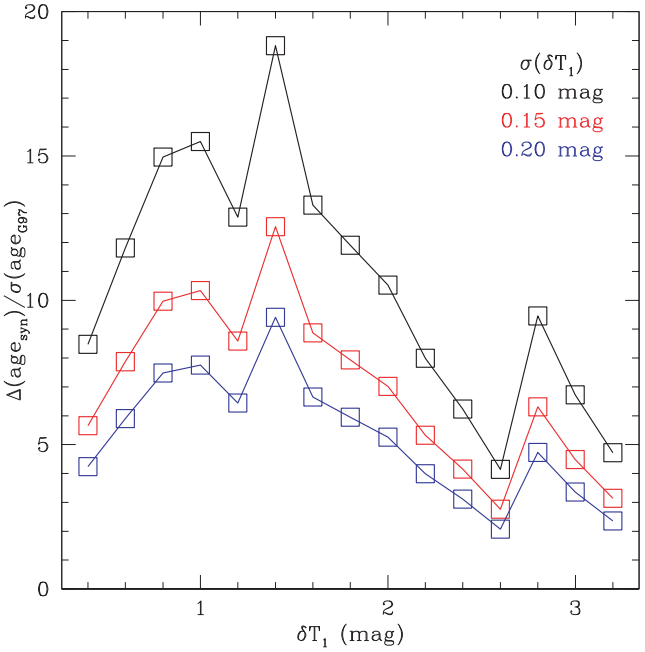

Figure 3. Synthetic age range of $\sigma(\text{age}_{G97})$ ratio as a function of δT_1.

hand, the older end of the G97 curve overlaps those of metal-poor clusters ([Fe/H] $\lesssim -1.5$ dex). The upper right-hand panel of Fig. 2 clearly illustrates this metallicity dependence of δT_1 for 12 different age levels. Indeed, for $\delta T_1 = 3.2$ mag an age of 10.3 Gyr is derived from the G97 calibration as well as from synthetic CMDs with [Fe/H] $\lesssim -1.5$ dex. However, a lower age of ∼2.5 Gyr is derived from synthetic CMDs if [Fe/H] > -1.0 dex is adopted. Such a difference between mean age values is statistically significant even if we consider an uncertainty of 0.15 mag in the δT_1 values. Similarly, for $\delta T_1 = 1.5$ mag, an age of 1.8 Gyr is derived from the G97 equation, or indistinctly from synthetic CMDs with [Fe/H] ≈−0.6 dex. Once again, if [Fe/H] values of −0.1 and −1.1 dex are used instead, the ages from synthetic CMDs would be 0.5 Gyr greater and 0.6 Gyr smaller than the G97 age, respectively; errors of 0.2 Gyr due to uncertainties in δT_1 were estimated.

The above examples not only illustrate that the δT_1 age index is sensitive to metallicity, but also that such a dependence is a complex function of both age and metallicity. Moreover, the age range for any particular δT_1 value obtained from the synthetic curves (see upper left-hand panel of Fig. 2) is many times larger than the age errors derived from equation (4) of G97. Fig. 3 illustrates this trend for three different δT_1 error levels. This result shows the need for a new calibration for the δT_1 age index to prevent any age/metallicity degeneracy.

We seek a straightforward relationship between the δT_1 values derived from synthetic cluster CMDs, the age and the metallicity. Bearing in mind the kind of arithmetic expressions employed in previous δ age calibrations (Phelps et al. 1994; Carraro & Chiosi 1994; Geisler et al. 1997; Salaris, Weiss & Percival 2004), we tried different possibilities, which included linear, quadratic and terms of higher degree for the three quantities, mixed terms, logarithmic functions, etc. Note that we used a larger number of points than any previous δ age calibration, uniformly distributed throughout the whole age/metallicity range and without any constraint from non-homogeneity in the age/metallicity values. Unfortunately, we did not attain any satisfactory fit, which confirms the complex interdependence of the three parameters.

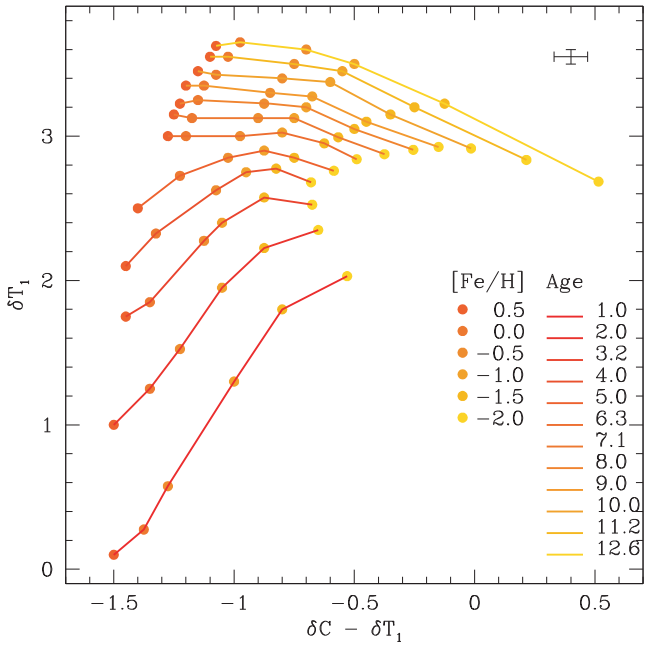

Figure 4. δT_1 versus $\delta C - \delta T_1$ diagram with iso-age lines and iso-metallicity loci. Metallicity and age labels are given in dex and Gyr, respectively.

To complement this analysis and by taking advantage of the availability of magnitudes in the C passband ($= T_1 + (C - T_1)$), Fig. 2 (bottom panels) also depicts the relationship for δC – defined as δT_1 but for the C filter – with the age and the metallicity. To build that relationship, we first produced synthetic C versus $C - T_1$ CMDs for the same synthetic clusters used to construct the top panels of Fig. 2. Then, we measured the magnitudes at the MSTO and the RC and computed their difference (δC). The resulting curves show that δC expands over a dynamical range of ∼4 mag, similar to that of δT_1. However, although the overall appearance of the δC and δT_1 curves is similar, the former show a less complex trend with age and metallicity. In particular, they do not account for: (i) the lack of metallicity sensitivity ([Fe/H] >-1.0 dex) for stellar populations older than ∼5 Gyr and (ii) the slope has changed for clusters more metal-poor than [Fe/H] $\lesssim -1.0$ dex. Nevertheless, Fig. 2 clearly suggests that δC is also a combined measurement of age and metallicity.

3.1 A new age–metallicity diagnostic diagram

At this point, we decided to introduce a new diagnostic diagram that can unambiguously provide age and metallicity estimates within certain Washington CT_1 photometric error limits. We found that the plane δT_1 versus $\delta C - \delta T_1$ was the best for distinguishing changes in age and metallicity throughout the whole two-dimensional space. In Fig. 4, we have traced iso-age lines and marked iso-abundance positions using colour-coded lines and filled circles, respectively. Error bars for typical uncertainties in δT_1 and $\delta C - \delta T_1$ are also indicated. Note that the iso-age lines and iso-metallicity positions rely on the theoretical isochrones used to build the synthetic CMDs, while the quoted errors refer to the uncertainty in measuring δC and δT_1 in observed cluster CMDs. In this sense, the capacity for resolving ages and metallicity varies with the position in that plane. Table 1 lists the age/metallicity errors associated with typical $\sigma(\delta T_1)$ and $\sigma(\delta C - \delta T_1)$ uncertainties, derived by interpolation of Fig. 4. In particular, we have highlighted in bold those errors for (age, [Fe/H]) pairs that are within the ranges of the age–metallicity relationships (AMRs) of the Milky Way and of the Small and Large Magellanic Clouds (Beasley et al. 2004; Sabbi et al. 2009; Piatti & Geisler 2013). Since star clusters can have ages and metallicities directly linked to the chemical evolution history (AMR) of their host galaxies, the highlighted age/metallicity ranges in Table 1 are more usable from an astrophysical point of view. We thickened the line sections in the δT_1 versus age diagram (see Fig. 5) corresponding to the age/metallicity values with uncertainties in Table 1 that are shown in bold. Thus, readers can consistently compare the G97 locus with the present theoretically driven calibration according to known AMRs. From Fig. 4, ($\delta C - \delta T_1$, δT_1) values can be used to obtain by interpolation age and metallicity estimates.

We used the new diagnostic diagram for clusters with high-quality CT_1 photometry, particularly with well-identified MSTOs and RCs, and with accurate ages and metallicities. We searched for metallicities obtained from high-dispersion spectroscopy, although in some cases we relaxed this requirement down to medium-dispersion spectroscopy or even to reliable photometric metal abundances. As for the cluster ages, we took advantage of those values derived from isochrones that were fitted to deep cluster CMDs. We excluded any previous age/metallicity estimates from Washington photometry.

Table 1. Estimated age (Gyr) and metallicity (dex) errors.[a]

[Fe/H]/ age	1.0	2.0	3.2	4.0	5.0	6.3
−2.0	0.20/0.15	0.20/0.20	0.30/0.20	0.50/0.25	0.70/0.20	0.80/0.25
−1.5	0.20/0.15	0.20/0.15	0.25/0.20	0.50/0.25	**0.60/0.25**	**0.70/0.25**
−1.0	**0.20/0.15**	**0.30/0.15**	**0.40/0.25**	**0.60/0.25**	**0.60/0.25**	**0.60/0.25**
−0.5	**0.20/0.15**	**0.25/0.15**	**0.40/0.25**	**0.50/0.20**	**0.50/0.25**	**0.50/0.25**
0.0	**0.15/0.20**	**0.15/0.20**	**0.20/0.20**	**0.40/0.20**	0.40/0.20	0.50/0.40
+0.5	**0.10/0.20**	0.10/0.20	0.20/0.20	0.30/0.20	0.30/0.20	0.40/0.50
[Fe/H]/ age	7.1	8.0	9.0	10.0	11.2	12.6
−2.0	0.60/0.20	0.60/0.15	0.70/0.15	0.70/0.15	**0.70/0.15**	**0.70/0.15**
−1.5	**1.00/0.20**	**1.00/0.15**	**1.00/0.15**	**1.00/0.15**	**1.00/0.15**	**1.00/0.15**
−1.0	**0.80/0.25**	**1.00/0.25**	**1.00/0.25**	**1.00/0.20**	**1.00/0.15**	**1.00/0.15**
−0.5	**0.50/0.20**	**0.70/0.20**	**0.70/0.20**	**0.60/0.20**	0.60/0.20	0.60/0.20
0.0	0.50/0.40	0.50/0.40	0.50/0.40	0.50/0.40	0.50/0.40	0.50/0.40
+0.5	0.80/0.50	0.80/0.50	0.80/0.50	0.80/0.50	0.80/0.50	0.80/0.50

Note. [a]Errors in age/metallicity were estimated using $\sigma(\delta C) = \sigma(\delta T_1) = 0.05$ mag and $\sigma(\delta C - \delta T_1) = [(\sigma C)^2 + (\sigma T_1)^2]^{1/2} = 0.07$ mag.

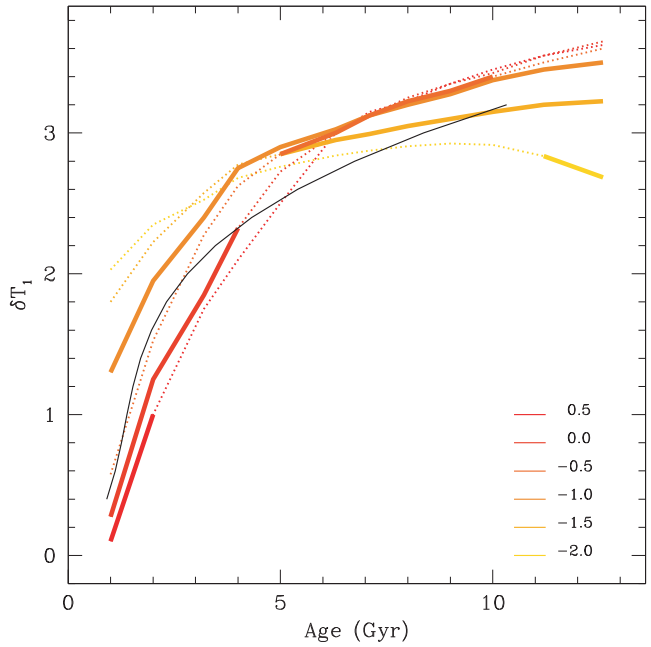

Figure 5. Same as Fig. 2 (upper left-hand panel), but thick line sections correspond to ages/metallicities with uncertainties shown in bold in Table 1.

From barely 340 clusters with published CT_1 data, we found nearly 150 with recognizable MSTOs and RCs. In general, the extracted cluster CMDs present signatures of contamination from the composite star field population along the line of sight. Such field contamination has a particular pattern given by the luminosity function, the colour distribution and the stellar density towards the cluster region. For these reasons, we first built CMDs representing the field along the line of sight towards the individual clusters, which we then used to clean the cluster CMDs with the aim of tracing fiducial cluster sequences as accurately as possible. We employed the cleaning procedure developed by Piatti & Bica (2012, see their fig. 12). The method compares the extracted cluster CMD to four distinct CMDs composed of stars located reasonably far from the object, but not too far to risk losing the local field–star signature in terms of stellar density, luminosity function and/or colour distribution. Each field region covers an equal area as that of the cluster and the four field areas are placed to the north, east, south and west from the cluster.

The comparison of the cluster/field CMDs is performed using boxes of different sizes distributed in the same manner throughout both CMDs, thus leading to a more meaningful comparison of the numbers of stars in different CMD regions than using boxes fixed in size and position. The latter is not universally efficient, since some parts of the CMD are more densely populated than others. For instance, to deal with stochastic effects at relatively bright magnitudes (e.g. fluctuations in the numbers of bright stars), larger boxes are required, while populous CMD regions can be characterized using smaller boxes. Since the procedure is executed for each of the four-field CMD box samples, it assigns a membership probability (P) to each star in the cluster CMD. This is done by counting the number of times a star remained unsubtracted in the four cleaning runs and by subsequently dividing this number by four. We used stars that are predominantly found in the cleaned cluster CMDs ($P \geq 75$ per cent).

We used the cleaned cluster CMDs to measure C and T_1 magnitudes at the MSTO and RC, then computed δC and δT_1 and used them with the age–metallicity diagnostic diagram to estimate cluster ages and metallicities. The resulting values with their uncertainties for clusters that fulfilled the requirements mentioned above (e.g. available age/metallicity values from independent Washington techniques) are listed in the last columns of Table 2, in which we also include age/metallicity values found by searching the literature thoroughly for comparison.

4 ANALYSIS

From the comparison between cluster ages taken from the literature and those estimated above (see Fig. 6), we obtained a mean age dispersion of $\Delta(\log(\mathrm{age yr}^{-1}) = 0.07 \pm 0.02$ along the whole age range (1–13 Gyr). The resulting mean dispersion is slightly smaller than typical age errors ($\Delta(\log(\mathrm{age yr}^{-1}) = 0.10$–$0.15$) derived from isochrone fitting to good-quality cluster CMDs, regardless of binarity, multiple populations, differential reddening, rotation effects, etc. This result shows that the age–metallicity diagnostic diagram returns accurate ages at low expense, since it does not require deep photometry nor does it deal with the known four-parameter degeneracy (age, metallicity, distance and reddening) when matching isochrones to the cluster CMDs. On the metallicity arena, the derived iron to hydrogen ratios are within $\Delta([\mathrm{Fe/H}]) = \pm 0.15$ dex of the identity relation (see Fig. 7) and no systematic dependence with the metallicity from the literature is visible along the considered range. Such a dispersion is also comparable to the smallest error attainable in deriving metal abundances from photometric data. The most discrepant point in Fig. 7 corresponds to NGC 6791, which is simply due to a drop in the metallicity sensitivity for metal-rich clusters older than 5 Gyr.

These results reveal that the diagnostic diagram is able to solve the constraints found in the δT_1 index, namely, the loss of age sensitivity for ages greater than ∼6 Gyr and the strong dependence on both age and metallicity for ages smaller than ∼5 Gyr. Indeed, as for metal-poor and old clusters, the loss of age sensitivity in δT_1 is surpassed when the $\delta C - \delta T_1$ index is used as a variable instead of the age as proposed by G97 (see top left-hand panel of Fig. 2). Such a choice can also be used to obtain a metallicity estimate. For ages younger than ∼5 Gyr, the diagnostic diagram shows that while δT_1 depends on the age and on the metallicity, $\delta C - \delta T_1$ is mainly a metal abundance indicator, so that the latter fixes the metallicity level when the former is evaluated.

In addition to the δT_1 age calibration, the M_{T_1} versus $(C - T_1)_o$ CMD was also calibrated in terms of metallicity by Geisler & Sarajedini (1999), who demonstrated the metallicity sensitivity of the standard giant branch (SGB, each giant branch corresponds to an iso-abundance curve) applicable to objects with ages $\gtrsim$5 Gyr; any age effects are small or negligible for such objects. However, the SGBs were defined for [Fe/H] <-0.5 dex using globular clusters older than 10 Gyr, so that it is important to examine as closely as possible the effect of applying such a calibration to much younger clusters. In view of the well-known age–metallicity degeneracy, Bica et al. (1998) explored this effect empirically by comparing SGB-based metallicities for 11 clusters with ages between 1 and 3 Gyr to standard values. They found a relatively constant offset of ∼0.4 dex; the SGB metallicities were underestimated due to the effects of age for clusters younger than ∼3 Gyr. Geisler et al. (2003) investigated this effect in much more detail using theoretical isochrones computed by Lejeune & Schaerer (2001) for two metallicity levels ([Fe/H] $= -1.3$ and -0.7 dex). They found that not only a constant offset of ∼0.4 dex but an exponential correction increasing towards younger ages is necessary. In particular, they adopted

Table 2. Cluster parameters taken from the literature and used for comparison .

Cluster	Age (Gyr)	Ref.	[Fe/H] (dex)	Ref.	CT_1 data Ref.	Age (Gyr) (this work)	[Fe/H] (dex) (this work)
47 Tuc	13.1 ± 0.9	1	−0.75 ± 0.04	11	15	13.0 ± 1.0	-0.80 ± 0.30
AM 3	4.9 ± 1.8	2	−0.8 ± 0.4	2	16	4.5 ± 0.7	−0.75 ± 0.40
ESO 121-SC03	9.0 ± 0.7	3	−0.93 ± 0.20	12	17	9.0 ± 1.0	−0.90 ± 0.30
HW 40	2.50 ± 0.35	2	−0.90 ± 0.15	2	16	3.0 ± 0.7	−1.00 ± 0.40
IC 2146	1.55 ± 0.05	4	−0.4 ± 0.2	4	18	1.5 ± 0.3	−0.60 ± 0.25
Lindsay 3	1.2 ± 0.3	2	−0.40 ± 0.15	2	19	1.3 ± 0.2	−0.50 ± 0.15
Lindsay 113	4.0 ± 0.7	2	−1.24 ± 0.11	2	20	3.5 ± 0.3	−1.20 ± 0.30
NGC 339	6.0 ± 0.5	5	−1.08 ± 0.12	5	16	5.2 ± 1.0	−1.00 ± 0.40
NGC 419	1.4 ± 0.2	6	−0.67 ± 0.12	13	21	1.3 ± 0.3	−0.75 ± 0.30
NGC 2682	4.2 ± 0.2	7	0.00 ± 0.06	14	15	4.2 ± 1.0	−0.10 ± 0.30
NGC 6791	7.0 ± 1.0	8	0.42 ± 0.05	14	15	7.5 ± 0.8	0.00 ± 0.50
SL 509	1.2 ± 0.2	9	−0.54 ± 0.09	9	17	1.0 ± 0.2	−0.40 ± 0.15
SL 862	1.7 ± 0.2	9	−0.47 ± 0.10	9	17	1.7 ± 0.4	−0.50 ± 0.25
Trumpler 5	3.0 ± 1.0	10	−0.40 ± 0.05	10	22	3.0 ± 0.5	−0.40 ± 0.15

References: (1) Roediger et al. (2014); (2) Dias et al. (2014); (3) Mackey, Payne & Gilmore (2006); (4) Milone et al. (2009); (5) Glatt et al. (2011); (6) Glatt et al. (2009); (7) Balaguer-Núñez, Galadí-Enríquez & Jordi (2007); (8) Anthony-Twarog et al. (2007); (9) Sharma et al. (2010); (10) Donati et al. (2015); (11) Bragaglia et al. (2010); (12) Olszewski et al. (1991); (13) Da Costa & Hatzidimitriou (1998); (14) Heiter et al. (2014); (15) Geisler & Sarajedini (1999); (16) Piatti (2011a); (17) Bica et al. (1998); (18) Piatti (2011b); (19) Piatti et al. (2011); (20) Piatti et al. (2007); (21) Piatti (2011c); (22) Piatti et al. (2004).

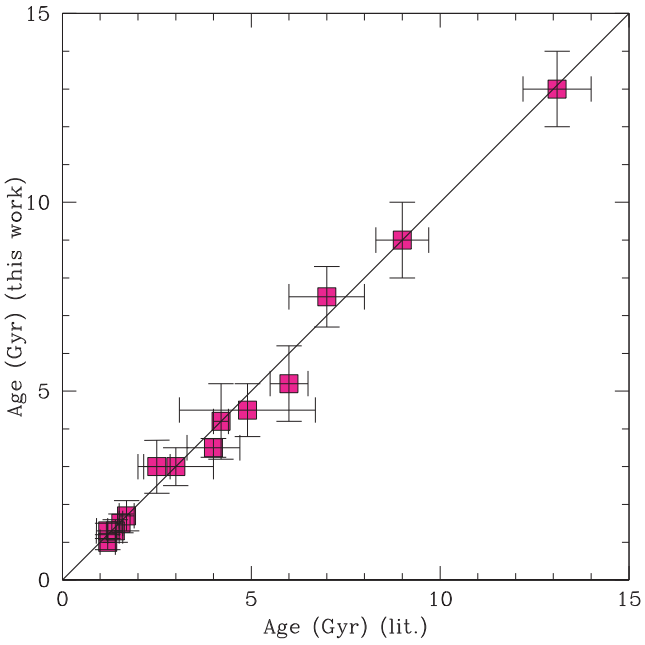

Figure 6. Comparison between ages taken from the literature and those estimated using the age–metallicity diagnostic diagram.

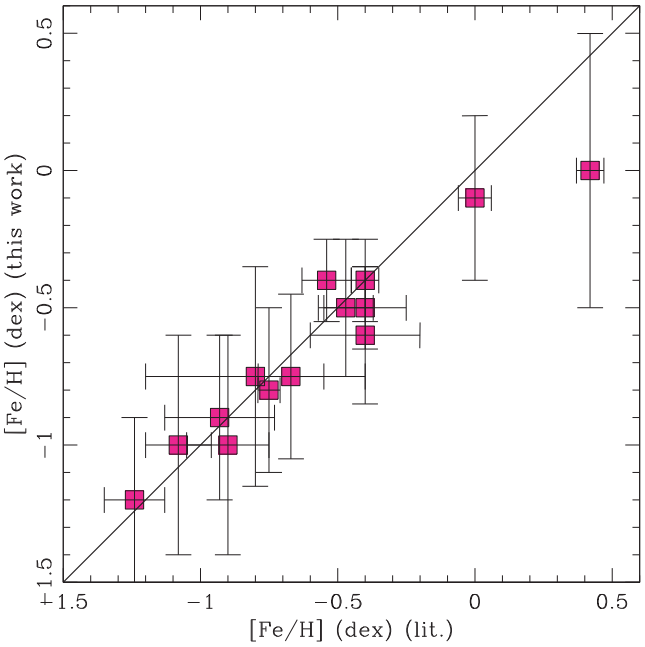

Figure 7. Comparison between metallicities taken from the literature and those estimated using the age–metallicity diagnostic diagram.

the theoretical prediction for [Fe/H] = −0.7 dex as the correction to be applied to the SGB metallicities as a function of age. Including all error sources, the corrected [Fe/H] values are estimated with an uncertainty of σ([Fe/H]) = 0.3 dex, although the steepness of the age correction for the youngest clusters (<2 Gyr) results in a larger metallicity error and biases the resulting metallicities upwards.

These successive improvements seem surpassed by the new age–metallicity diagnostic diagram. The latter can be used without knowledge of the cluster distance and reddening, which is mandatory in the SGB technique. Likewise, the diagnostic diagram can not only be used to estimate directly more precise metallicities but also ages, simultaneously. The new procedure requires no correction and is useful for a wide range of ages (1–13 Gyr) and metallicities ([Fe/H] = −2.0–+0.5 dex). All these features make the diagnostic diagram a powerful tool for estimating accurate ages as well as metallicities.

5 CONCLUSIONS

The Washington photometric system has long been used to estimate ages and metallicities of clusters, particularly for those older than ∼1 Gyr. Nevertheless, these estimates have relied on

calibrations (δT_1 and SGB methods), which involve clusters with ages and metallicities that need to be updated. Likewise, the well-known age–metallicity degeneracy has not been properly addressed or sometimes not even considered at all.

We have profusely exploited synthetic T_1 versus $C - T_1$ CMDs with the aim of improving our knowledge about the intrinsic behaviour of the δT_1 index with age and metallicity. The synthetic CMDs were produced through the ASTECA suite of functions, taking into account the total cluster mass as a function of age to give MSTO and RC similarly populated to the known low-mass clusters. Photometric errors were also considered, so that the resulting cluster CMDs achieved the appearance of the observed ones.

The analysis of the δT_1 index as a function of age for different metallicity levels shows that it varies with age and metal content as well. In general, the dependence on age weakens for ages greater than $\sim$6 Gyr, and is even less sensitive to age as the metallicity decreases ([Fe/H] $\lesssim -1.0$ dex). For ages younger than $\sim$5 Gyr, δT_1 shows a strong correlation with both age and metallicity. As expected, the δC index – defined as δT_1 for the C passband – is also a combined measurement of age and metallicity.

We introduce a new age–metallicity diagnostic diagram, δT_1 versus $\delta C - \delta T_1$, which has been shown to unambiguously provide age and metallicity estimates, simultaneously, within certain Washington CT_1 photometric error limits. The proposed technique does not require any additional measurement from other Washington passbands, but only the same CT_1 photometry needed to measure the former δT_1 index. The new procedure can be used to derive ages and metallicities within a considerable wide range (age: 1–13 Gyr, [Fe/H]: -2.0–$+0.5$ dex), and is independent of the cluster reddening and distance modulus. It solves the constraints of the δT_1 index and surpasses the performance of the SGB method.

ACKNOWLEDGEMENTS

This work was partially supported by the Argentinian institutions CONICET and Agencia Nacional de Promoción Científica y Tecnológica (ANPCyT). We are grateful for the comments and suggestions raised by the anonymous referee, which helped us to improve the manuscript.

REFERENCES

Anthony-Twarog B. J., Twarog B. A., Mayer L., 2007, AJ, 133, 1585
Balaguer-Núñez L., Galadí-Enríquez D., Jordi C., 2007, A&A, 470, 585
Baumgardt H., Parmentier G., Anders P., Grebel E. K., 2013, MNRAS, 430, 676
Beasley M. A., Brodie J. P., Strader J., Forbes D. A., Proctor R. N., Barmby P., Huchra J. P., 2004, AJ, 128, 1623
Bica E., Geisler D., Dottori H., Clariá J. J., Piatti A. E., Santos J. F. C., Jr, 1998, AJ, 116, 723
Bragaglia A., Carretta E., Gratton R., D'Orazi V., Cassisi S., Lucatello S., 2010, A&A, 519, A60
Bressan A., Marigo P., Girardi L., Salasnich B., Dal Cero C., Rubele S., Nanni A., 2012, MNRAS, 427, 127
Canterna R., 1976, AJ, 81, 228
Carraro G., Chiosi C., 1994, A&A, 287, 761
Casagrande L., VandenBerg D. A., 2014, MNRAS, 444, 392
Catelan M., Leyton P. P., Saito R. K., Borissova J., Popescu B., 2014, in Revista Mexicana de Astronomia y Astrofisica, Vol. 44, Revista Mexicana de Astronomia y Astrofisica Conference Series, p. 65
Chabrier G., 2001, ApJ, 554, 1274
Correnti M., Goudfrooij P., Kalirai J. S., Girardi L., Puzia T. H., Kerber L., 2014, ApJ, 793, 121
Da Costa G. S., Hatzidimitriou D., 1998, AJ, 115, 1934
de Grijs R., Goodwin S. P., Anders P., 2013, MNRAS, 436, 136
Dias B., Kerber L. O., Barbuy B., Santiago B., Ortolani S., Balbinot E., 2014, A&A, 561, A106
Donati P., Cocozza G., Bragaglia A., Pancino E., Cantat-Gaudin T., Carrera R., Tosi M., 2015, MNRAS, 446, 1411
Geisler D., Sarajedini A., 1999, AJ, 117, 308
Geisler D., Bica E., Dottori H., Claria J. J., Piatti A. E., Santos J. F. C., Jr, 1997, AJ, 114, 1920 (G97)
Geisler D., Piatti A. E., Bica E., Clariá J. J., 2003, MNRAS, 341, 771
Glatt K. et al., 2009, AJ, 138, 1403
Glatt K. et al., 2011, AJ, 142, 36
Heiter U., Soubiran C., Netopil M., Paunzen E., 2014, A&A, 561, A93
Hernandez X., Valls-Gabaud D., Gilmore G., 1999, MNRAS, 304, 705
Jiang D., Han Z., Li L., 2014, ApJ, 789, 88
Kerber L. O., Girardi L., Rubele S., Cioni M.-R., 2009, A&A, 499, 697
Kroupa P., 2002, Science, 295, 82
Kroupa P., Tout C. A., Gilmore G., 1993, MNRAS, 262, 545
Lejeune T., Schaerer D., 2001, A&A, 366, 538
Li Z., Mao C., Chen L., Zhang Q., 2012, ApJ, 761, L22
Li C., de Grijs R., Deng L., 2013, MNRAS, 436, 1497
Mackey A. D., Payne M. J., Gilmore G. F., 2006, MNRAS, 369, 921
Milone A. P., Bedin L. R., Piotto G., Anderson J., 2009, A&A, 497, 755
Monteiro H., Dias W. S., Caetano T. C., 2010, A&A, 516, A2
Olszewski E. W., Schommer R. A., Suntzeff N. B., Harris H. C., 1991, AJ, 101, 515
Perren G. I., Vázquez R. A., Piatti A. E., 2015, A&A, 576, 6
Phelps R. L., Janes K. A., Montgomery K. A., 1994, AJ, 107, 1079
Piatti A. E., 2011a, MNRAS, 416, L89
Piatti A. E., 2011b, MNRAS, 418, L40
Piatti A. E., 2011c, MNRAS, 418, L69
Piatti A. E., 2014, MNRAS, 437, 1646
Piatti A. E., Bica E., 2012, MNRAS, 425, 3085
Piatti A. E., Geisler D., 2013, AJ, 145, 17
Piatti A. E., Santos J. F. C., Clariá J. J., Bica E., Sarajedini A., Geisler D., 2001, MNRAS, 325, 792
Piatti A. E., Bica E., Geisler D., Clariá J. J., 2003, MNRAS, 344, 965
Piatti A. E., Clariá J. J., Ahumada A. V., 2004, MNRAS, 349, 641
Piatti A. E., Sarajedini A., Geisler D., Gallart C., Wischnjewsky M., 2007, MNRAS, 381, L84
Piatti A. E., Clariá J. J., Bica E., Geisler D., Ahumada A. V., Girardi L., 2011, MNRAS, 417, 1559
Piatti A. E., Geisler D., Mateluna R., 2012, AJ, 144, 100
Popescu B., Hanson M. M., 2014, ApJ, 780, 27
Popescu B., Hanson M. M., Elmegreen B. G., 2012, ApJ, 751, 122
Roediger J. C., Courteau S., Graves G., Schiavon R. P., 2014, ApJS, 210, 10
Romeo G., Fusi Pecci F., Bonifazi A., Tosi M., 1989, MNRAS, 240, 459
Rubele S. et al., 2012, A&A, 537, A106
Sabbi E. et al., 2009, ApJ, 703, 721
Salaris M., Weiss A., Percival S. M., 2004, A&A, 414, 163
Sharma S., Borissova J., Kurtev R., Ivanov V. D., Geisler D., 2010, AJ, 139, 878
Suntzeff N. B., Schommer R. A., Olszewski E. W., Walker A. R., 1992, AJ, 104, 1743
von Hippel T., 2005, ApJ, 622, 565

This paper has been typeset from a TEX/LATEX file prepared by the author.